Design of gain schedule fractional PID control for nonlinear thrust vector control missile with uncertainty

Mohamed Fawzy Ahmed & Hassen Taher Dorrah

Published online: 28 Nov 2018.

Submit your article to this journal

Article views: 695

View related articles

View Crossmark data

Taylor & Francis
Taylor & Francis Group

REGULAR PAPER

Design of gain schedule fractional PID control for nonlinear thrust vector control missile with uncertainty

Mohamed Fawzy Ahmed and Hassen Taher Dorrah

Faculty of Engineering, Cairo University, Giza, Egypt

ABSTRACT

The purpose of this paper is to control the trajectory of the nonlinear missile model in the pitch channel by using Fractional *PID* controller (*FPID*) and Gain Schedule Fractional *PID* controller (*GSFPID*). *FPID* and *GSFPID* with nonlinear missile model are designed where their parameters are tuned by Simulink design optimization in the Matlab toolbox. This optimization method gives the optimal parameters that achieve the best tracking with step unit reference signal. The *GSF-PID* controller compensates the restrictions that represent physical limits of actuators in the pitch channel. The *GSFPID* with nonlinear missile model is designed in two phases. The first phase is the boost phase where the thrust force is maximized and the second phase is sustain phase where the thrust force is minimized. The equations of motion for nonlinear missile model with *FPID* and *GSFPID* are modelled mathematically in the Matlab-Simulink environment. The results of *FPID* and *GSFPID* controllers with the nonlinear missile model are presented and compared. The wind effect and the dynamic uncertainties effects are researched and the results are compared. The closed-loop nonlinear system is linearized by the Simulink linear analysis tool at critical operating point $t = 5.8$ sec and the stability is studied.

1. Introduction and literature review

The quality requirements for automatic control have increased due to the great complication for plants and the increasingly complicated properties for production. The controllers with a six degree of freedom (6-*DOF*) missile model in pitch channel will be addressed in this paper. The 6-*DOF* missile model gives true information about the missile path. The purpose of this paper:

(1) To develop a complicated mathematical model of flying path simulation for a missile in pitch channel. This mathematical model is utilized as an algorithm for designing, analysis, and development of the framework to present the missile motion by the Simulink environment to ease the design of the control structure.

(2) According to the system features and application environment required, *GSFPID* control strategy is proposed to solve the missile attitude control problem. *GSFPID* controller compensates the restrictions that represent physical limits of actuators in the pitch channel. The dynamic uncertainties are studied where the aerodynamic coefficients of the missile are changed to study the robustness [1,2]. The closed-loop nonlinear system is linearized by the Simulink linear analysis tool at critical operating point $t = 5.8$ sec to study the stability system by the Nyquist diagram and Bode diagram.

In this paper, the autopilot is equipped with thrust vector control that does not depend on the dynamic pressure of the atmosphere. Hence, the thrust force and thrust moment change the motion behaviour of the missile, [3]. The missile system operates in two phases; the first phase is the boost phase where the thrust force is maximized. The second phase is the sustain phase where the thrust force is minimized [1,2]. *FPID* and *GSFPID* controllers' gains with nonlinear missile model are tuned by Simulink design optimization.

According to *MacKenzie*, guidance is defined as the procedure for guiding the path of an object toward a given point [1,4]. Moreover, *Charles Stark Draper* stated that Guidance depends on main basics and includes vehicles steering in different environments beyond the atmosphere with the gravitational field and in space [1,5]. The most wealthy and ripe for guidance is established with the steering missile. A guided missile is defined as a space-navigating unmanned vehicle that carries within itself the means for controlling its flying route [1,6]. Guided missiles are operated since World War II [1,4]. Today, missile control method involves a wide field of steering laws such as traditional control, optimal control, fuzzy logic and neural network control and differential geometric control rules. The steering missile evolution through and after World War II are found in the following literature [1,7–9]. Moreover, *Locke and Westrum* placed the evolution of steering missile methods into a great view [1,10,11].

At the end of the nineteeth century, the initial definition of the fractional derivative was introduced by *Liouville* and *Riemann*. However, this idea started to be enjoyable for engineers in the late 1960s, especially when it was seen that the characteristic of some systems is more precise when the fractional derivative is utilized. There are increasing numbers of implementation of the fractional calculus such as the use of fractional order controllers, like the *FPID* ($PI^\lambda D^\delta$) controller [12]. The $PI^\lambda D^\delta$ controller has both the differentiation and integration of fractional order, which awards the ability to adjust control systems. The *FPID* controller that is utilized in the path-tracking trouble of the vehicle industry is given in [13]. Fractional order algorithms that are used in the hybrid control of robotic manipulators are observed in [14].

The novelty of the contribution of this paper can be summarized as follows

(1) The main contribution is using the gain schedule design with fractional order calculus controller for the first time.
(2) The Simulink design optimization method is used to tune the controller parameters with nonlinear missile model to improve the tracking performance.
(3) *GSFPID* control can achieve superior performance and effectiveness by comparing it with *FPID* control.
(4) The robustness of the proposed control (*GSFPID*) is validated by simulation results where the wind disturbance effect and dynamic uncertainties will be studied.
(5) The stability of the proposed control (*GSFPID*) is researched by using the Nyquist stability diagram and Bode diagram.

The rest of this paper is organized as follows. Section 2 represents the mathematical model of 6-*DOF* for the missile. Section 3 displays Gain Schedule *FPID* controller design for pitch channel of nonlinear missile model. Section 4 presents control implementation and outcomes. Finally, conclusions and future work are discussed in section 5.

2. Mathematical model of 6-DOF for missile

The 6-*DOF* equations for nonlinear missile model are divided into depicting kinematics, dynamics (thrust, gravity and aerodynamic), leading guidance descent model, and autopilot (electronics, actuators, and instruments). The inputs of the model are the initial situations, target movement, and target path description. The outputs of the model are the missile flying description (missile velocity and attitude angles).

This paper discusses the autopilot of a missile equipped with thrust vector control (*TVC*). This method of control does not rely on the dynamic pressure of the atmosphere but it is based on motor thrust. The variation of the thrust vector depends on the control demand. Hence, thrust force and thrust moment change the motion behaviour of the missile. It allows for the variation of the direction of the thrust vector with respect to the symmetry axes of the missile. Thrust vector control has been seen for many missile engines using solid or liquid propellants. The missile can fly in the desired attitude utilizing the thrust vector control [3,15,16]. The essential framing required for mathematical evolutions are the body, velocity and ground coordinates. The origin of these coordinates is the center of gravity (*c.g*) for the missile. In the ground coordinate system, the $X_g - Z_g$ is the horizontal plane and the Y_g axis complements a standard right-handed system and goes up perpendicularly. In the body coordinate, the positive X_b axis corresponds to the center line of the missile and presents the roll-axis. The positive Z_b axis is vertical to the X_b axis in the horizontal surface and presents the pitch axis. The positive Y_b axis goes up and presents the yaw axis. The body axis system is constant with the missile and gets about with it. In the velocity coordinate, X_V corresponds to the direction of missile speed (V_m) that is linked to the direction for missile flying. The axis Z_V supplements a standard right-handed system [1,2,17–19].

The pitch plane is $X–Y$ surface, the yaw plane is $X–Z$ surface, and the roll plane is $Y–Z$ surface. The ground coordinate and body coordinate are linked to each other through attitude angles (Ψ, Φ, Υ). The ground coordinate and velocity coordinate are linked to each other through the angles(θ, σ). The velocity coordinate system is linked to the body frame through the angle of attack (α) in the pitch plane and sideslip angle (β) in the yaw plane. The angles between various coordinate systems are represented in Figure 1 [1,2,17,19,20]. The relationship between the velocity and the body coordinate systems can be obtained as follows:

$$\begin{bmatrix} X_b \\ Y_b \\ Z_b \end{bmatrix} = \begin{bmatrix} \cos(\beta)\cos(\alpha) & \cos(\beta)\sin(\alpha) & -\sin(\beta) \\ -\sin(\alpha) & \cos(\alpha) & 0 \\ \sin(\beta)\cos(\alpha) & \sin(\beta)\sin(\alpha) & \cos(\beta) \end{bmatrix}$$
$$\times \begin{bmatrix} X_v \\ Y_v \\ Z_v \end{bmatrix} \quad (1)$$

The velocity and body axes system, as well as moments, forces and other quantities are shown in Figure 2.

There are six kinematic equations (three for rotational movement and three for translational movement) and six dynamic equations (three for rotational movement and three for translation movement) for 6-*DOF* missile. The missile 6-*DOF* equations are obtained as shown, [1,2,19–21].

$$F_x = m\dot{V}_m \quad (2)$$

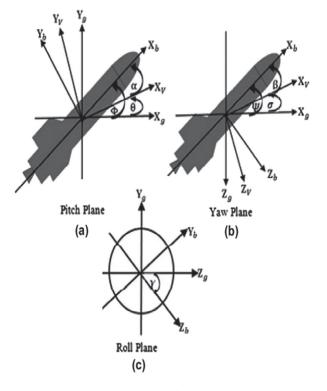$$\dot{\Psi} = (\omega_y \cos(\Upsilon) - \omega_z \sin(\Upsilon)) / \cos(\Phi) \tag{11}$$

$$\dot{\Phi} = \omega_y \sin(\Upsilon) + \omega_z \cos(\Upsilon) \tag{12}$$

$$\dot{\Upsilon} = \omega_x - \tan(\Phi)(\omega_y \cos(\Upsilon) - \omega_z \sin(\Upsilon)) \tag{13}$$

$$\dot{\alpha} = \dot{\Phi} - \dot{\theta} \tag{14}$$

$$\dot{\beta} = \dot{\Psi} - \dot{\sigma} \tag{15}$$

In these equations, M_x, M_y, M_z are moments represented in body coordinate [N.m]; F_x, F_y, F_z are component of forces represented in velocity coordinate [N]; I_x, I_y, I_z are moments of inertia in body coordinate [kg.m^2]; ω_x, ω_y, ω_z are angular velocity in body coordinate [rad/sec]; X is missile range [m]; Z is missile horizontal displacement [m]; Y is missile altitude [m]; and m is mass of missile [kg]. The moments and the forces present on the missile due to gravity, aerodynamic and thrust. These moments and forces are obtained as follows [1,2,17,19,20,22].

$$F_x = T \cos(\alpha - \delta_\alpha) \cos(\beta - \delta_\beta)$$
$$- QS(C_{x0} + C_x(\alpha^2 + \beta^2)) - mg \sin(\theta) \tag{16}$$

$$F_y = T \sin(\alpha - \delta_\alpha) + QSC_y\alpha - mg \cos(\theta) \tag{17}$$

$$F_z = -T \cos(\alpha - \delta_\alpha) \sin(\beta - \delta_\beta) - QSC_z\beta \tag{18}$$

$$M_x = DQSm_{x0} \frac{\omega_x D}{2V_m} \tag{19}$$

$$M_y = -T \cos(\delta_\alpha) \sin(\delta_\beta) X_{cg}$$
$$+ DQS \left(m_{y\beta}\beta + m_{y0} \frac{\omega_y D}{V_m} \right) \tag{20}$$

$$M_z = T \sin(\delta_\alpha) X_{cg} + DQS \left(m_{z\alpha}\alpha + m_{z0} \frac{\omega_z D}{V_m} \right) \tag{21}$$

In these equations, $m_{x0}, m_{y\beta}, m_{y0}, m_{z\alpha}, m_{z0}$ are aerodynamic moment coefficients [dimensionless]; C_x, C_{x0}, C_y, C_z are aerodynamic force coefficient [dimensionless]; S is the reference area [m^2]; D is the maximum cross section diameter of body [m]; Q is the dynamic pressure [kg/m.sec^2]; δ_α is the pitch nozzle deflection angle [º]; δ_β is the yaw nozzle deflection angle [º]; T is the thrust force [N]; X_{cg} is the dimension between the nozzle and center of gravity (c.g) [m]; and g is gravity acceleration constant 9.81 m/sec^2.

In this paper, the attitude control structure is designed in the pitch channel (X–Y plane), the yaw and roll channels are neglected. The nonlinear equations of

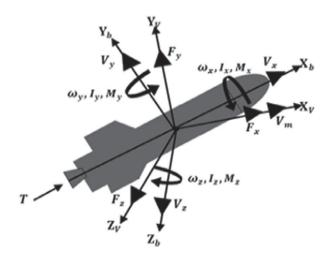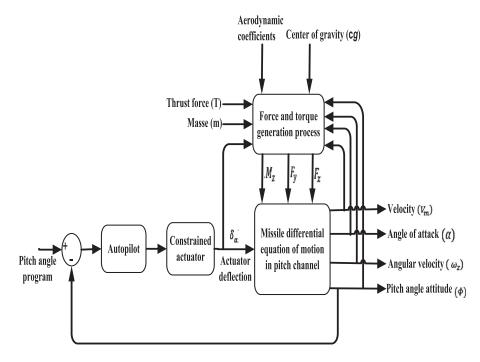**Figure 1.** The angles between different coordinate systems.

Figure 2. Moments, forces and other quantities.

$$F_y = mV_m\dot{\theta} \tag{3}$$

$$F_z = -mV_m \cos(\theta) \dot{\sigma} \tag{4}$$

$$M_x = I_x\dot{\omega}_x - (I_y - I_z)\omega_y\omega_z \tag{5}$$

$$M_y = I_y\dot{\omega}_y - (I_z - I_x)\omega_z\omega_x \tag{6}$$

$$M_z = I_z\dot{\omega}_z - (I_x - I_y)\omega_x\omega_y \tag{7}$$

$$\dot{X} = V_m \cos(\theta) \cos(\sigma) \tag{8}$$

$$\dot{Y} = V_m \sin(\theta) \tag{9}$$

$$\dot{Z} = -V_m \cos(\theta) \sin(\sigma) \tag{10}$$

Figure 3. Block diagram of pitch angle attitude control.

motion in the pitch channel are presented as follows [23–25].

$$\dot{\Phi} = \omega_z \qquad (22)$$

$$\dot{\alpha} = \omega_z - \frac{F_y}{mV_m} = -\frac{QSC_y}{mV_m}\alpha - \frac{T}{mV_m}\sin(\alpha - \delta_\alpha)$$
$$+ \omega_z + \frac{g}{V_m}\cos(\theta) \qquad (23)$$

$$\dot{\omega}_z = \frac{M_z}{I_z} = \frac{QSDm_{z\alpha}}{I_z}\alpha + \frac{QSD^2 m_{z0}}{I_z V_m}\omega_z$$
$$+ \frac{TX_{cg}}{I_z}\sin(\delta_\alpha) \qquad (24)$$

The block diagram of pitch angle attitude control is depicted in Figure 3

3. Gain schedule *FPID* controller design for pitch channel of nonlinear missile model

The researchers stated that controllers utilize fractional order derivatives and integrals to realize performance and robustness outputs those got with classic (integer order) controllers. The Fractional-order *PID* controller (*FPID*) controller is the expansion of the classic *PID* controller depends on fractional calculus. The theories of fractional calculus are explained in [1].

3.1. Basic concepts of FPID controller PI^λD^δ

The differential equation of the $PI^\lambda D^\delta$ controller is depicted in the time domain by:

$$u(t) = k_p e(t) + k_i D_t^{-\lambda} e(t) + k_d D_t^\delta e(t) \qquad (25)$$

The continuous transfer function of the $PI^\lambda D^\delta$ controller is given through Laplace transform

$$G_c(s) = k_p + k_i s^{-\lambda} + k_d s^\delta \qquad (26)$$

The *FPID* controller not only wants to design 3 parameters k_p, k_i and k_d, but also design 2 fractional orders λ, δ of integral and derivative controllers. The orders λ and δ are not necessarily integers but any real numbers, [1,26].

3.2. Optimal tuning FPID control parameters by Simulink design optimization

Tuned *FPID* controller with actuator restrictions is implemented in the Matlab using Simulink design optimization software that is named the nonlinear control design block set (*NCD*) [27,28]. This software has characteristics to optimize the design standard in any Simulink model by tuning required parameters that have natural actuation boundaries. Rise time, settling time, overshoot, and saturation limits are design requirements in Simulink response optimization. The gradient descent optimization method is selected to get the optimal *FPID* parameters. The gradient descent is the simplest method for optimization. The gradient descent method is explained in [3,26,29].

Simulink Design Optimization software gets gains that permit a proper solution with the given restrictions. Once the appropriate signals are constrained with signal limits the adjusted gains are set, and optimization tuning is given, the optimization is ready to run. Simulink Design Optimization software initials by drawing the starting response in blue in the Signal Constraint window. Through the optimization,
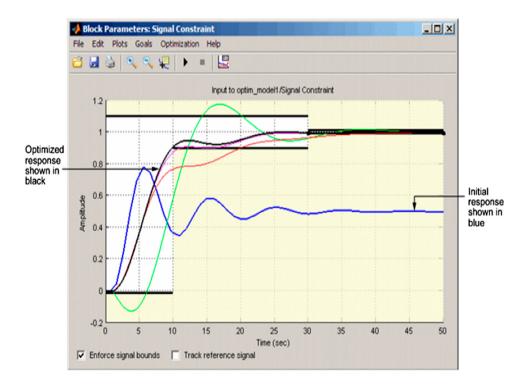
Figure 4. Simulink design optimization procedures.

the responses are drawn in different colours. The end response is drawn in black. Simulink Design Optimization software modifies the tuning gains within the Matlab workspace and depicts the parameter values in the Optimization Progress window. Figure 4 displays Simulink Design Optimization procedures [3,28,30].

FPID controller is designed with actuator restrictions so deviation response of the actuator and closed-loop system meets the given constraints for tracking. *FPID* parameters, that are tuned, are *kd* (derivative gain), *ki* (integral gain), *kp* (proportional gain), λ (fractional order of integral gain) and δ (fractional order of derivative gain) [3,26,28,30].

3.3. Gain scheduling controller

In many situations, the dynamics of plants are varied with the operating conditions of the process. It is possible to vary the parameters of the controller by seeing the operating conditions of the process. This technique is called gain scheduling. Gain scheduling is simple to process in computer controlled systems. Gain scheduling depends on measurements of procedures of the process and it is the best way to compensate for varying process parameters or unknown nonlinearities. If the familiar definition of the adaptive controller is utilized, Gain schedule is a very helpful procedure for decreasing the effects of parameter variations. There are several commercial process control systems that utilize gain schedule to compensate for dynamic and static nonlinearities. It is possible to decrease the effects of parameter variations by varying the parameters of the controller as functions of the additional variables.
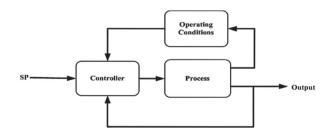

Figure 5. General block diagram of gain scheduled controller.

Gain scheduling can be got as a feedback control system where the feedback gains are tuned by utilizing feedforward compensation. The essential problem in the design of systems with gain scheduling is to obtain appropriate scheduling variables. This is done by the information basis of the system. When scheduling variables are obtained, the controller parameters are calculated at a number of operating points. The controller is adjusted for each operating point. The stability and performance of the system are obtained by simulation [31–35]. The general block diagram of the gain schedule controller is shown in Figure 5.

4. Control implementation and outcomes

In this section, the path of 6-*DOF* flight body model in pitch channel is controlled by *GSFPID* controller. *GSFPID* controller is designed where their parameters are tuned by Simulink Design Optimization. The equation of motion for the nonlinear flying body with *GSFPID* controller is modelled mathematically in the Matlab-Simulink environment. The results of nonlinear flying body model with *GSFPID* will be given and compared

with the results of the nonlinear flying body with *FPID* [1,11,20,36].

4.1. Nonlinear missile model description

Missile solid propellant thrust will be branched into 2 main phases:

(1) Boost phase: At time 0–5.8 sec and thrust force is maximized.
(2) Sustain phase: At time 5.8–25 sec and thrust force is minimized.

The deflection angle of the pitch actuator (δ_α) is limited with $\pm 22.9°$ (± 0.4 rad). The thrust force curve is represented in Figure 6.

Missile mass will be divided into two types according to variation with time:

(1) Constant with time: That includes missile frame, the actuation system, gyroscope and electrical package.
(2) Variable with time: That includes missile solid propellant with boost and sustains phases, igniter, and wire dispensing.

$$\dot{m}_{boost} = \frac{m_{boost}}{t_{boost}} \quad (27)$$

$$\dot{m}_{sustain} = \frac{m_{sustain}}{t_{sustain}} \quad (28)$$

$$\dot{m}_{var} = \frac{m_{var}}{t_{flight}} \quad (29)$$

$$m_{var} = m_{wire} + m_{igniter} \quad (30)$$

$$t_{flight} = t_{boost} + t_{sustain} \quad (31)$$

where: m_{boost} is the propellant mass during boost phase [kg]; t_{boost} is the boost time (0–5.8 sec); $m_{sustain}$ is the propellant mass during sustain phase
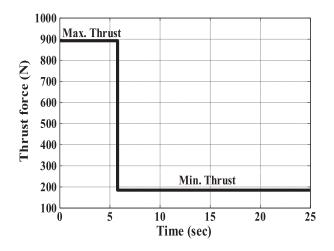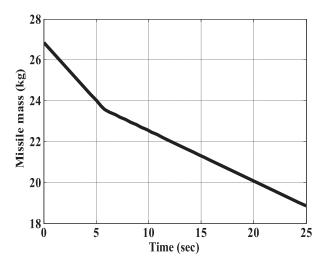

Figure 6. Thrust force curve.

Figure 7. Missile body and variable propellant mass curve.

[kg]; $t_{sustain}$ is the sustain time (5.8–25 sec); t_{flight} is the total flight time; m_{wire} is the wire dispenser mass [kg]; $m_{igniter}$ is the igniter mass [kg]; m_{var} is the variable mass (igniter and wire mass) [kg]; $\dot{m}_{boost}$ is the propellant burning rate during boost phase [kg/sec]; $\dot{m}_{sustain}$ is the propellant burning rate during sustain phase [kg/sec]; $\dot{m}_{var}$ is the wire dispensing rate and igniter burning rate [kg/sec]. The missile mass varies with time and is given as follows:

$$m = \begin{cases} m_0 - (\dot{m}_{boost} + \dot{m}_{var})t & 0 \le t < 5.8 \\ m_0 - m_{boost} & \\ -\dot{m}_{sustain}(t - t_{boost}) - \dot{m}_{var}t & 5.8 \le t < 25 \end{cases} \quad (32)$$

where: m_0 is the initial missile body mass and the initial propellant mass [kg]; m is the missile mass and variable propellant mass [kg]. Figure 7 depicts the missile body and variable propellant mass curve.

The aerodynamic force and moment coefficients are usually allocated in the form of graphs obtained by experiments in wind tunnel. Aerodynamic coefficients are represented as a function of Mach number that is varied with missile velocity (V_m). All aerodynamic coefficients are dimensionless. Figure 8 shows the drag force coefficient at zero angle of attack (C_{x0}). Drag force coefficient due to the angle of attack (C_x) is shown in Figure 9.

Lateral force coefficient (C_y) is displayed in Figure 10. The aerodynamic damping moment coefficient (m_{z0}) is depicted in Figure 11. Figure 12 demonstrates the aerodynamic moment coefficient.

4.2. Controller design

The *FPID* controller has 5 tuning parameter k_p, k_i, k_d, λ and δ which are tuned by Simulink Design Optimization through signal constraint that was explained in
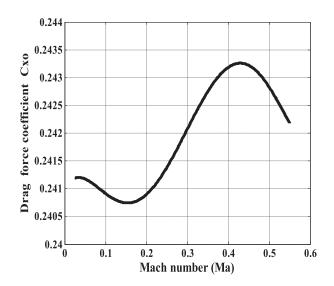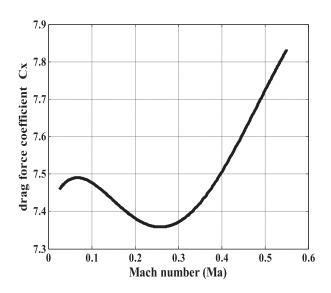
Figure 8. Drag force coefficient at zero angle of attack.
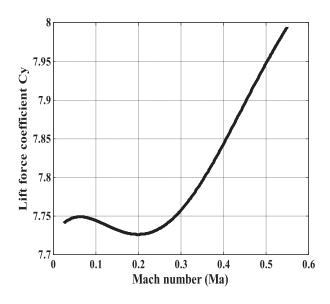

Figure 9. Drag force coefficient.

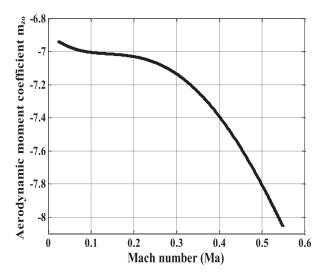**Figure 10.** Lateral force coefficient.

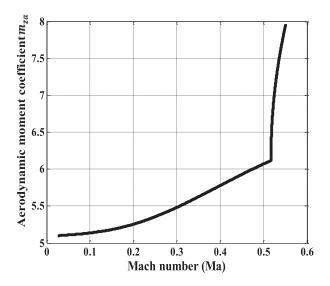**Figure 11.** The aerodynamic damping moment coefficient.

Figure 12. The aerodynamic moment coefficient.

section 3. The two *FPID* controllers are used in the *GSFPID* control. The first is tuned with boost phase ($0 \leq t < 5.8$ sec) but the second is tuned with sustain phase ($5.8 \leq t < 25$ sec). The optimized parameters of the *FPID* controller are shown in Table 1.

The optimized parameters of *GSFPID* controller at boost phase ($0 \leq t < 5.8$ sec) are seen in Table 2.

The optimized parameters of gain schedule *FPID* controller at sustain phase ($5.8 \leq t < 25$ sec) are seen in Table 3.

Table 1. The optimized parameters of *FPID* controller.

k_p	k_i	λ	k_d	δ
18.47	29.9	0.943	4.709	0.6608

Table 2. The optimized parameters of *GSFPID* controller at boost phase.

k_p	k_i	λ	k_d	δ
21.934	91.4234	0.9241	0.3592	0.949

Table 3. The optimized parameters of *GSFPID* controller at sustain phase.

k_p	k_i	λ	k_d	δ
155.0734	261.7472	1.0808	298.509	0.244

4.3. Simulation results

In this section, *FPID* and *GSFPID* controllers are designed in pitch channel with step unit reference signal where its initial value is 40° (0.698 *rad*) and its final value at first second is 41° (0.716 *rad*).

Figure 13 gives simulink diagram of nonlinear dynamic system with *GSFPID* in pitch channel. Figure 14 displays a block diagram of nonlinear dynamic system with *GSFPID* in pitch Channel.

Figure 15 represents pitch angle (plant output) comparison between *FPID* and *GSFPID* for nonlinear model.

Figure 16 depicts the pitch error (the difference between the step unit reference signal and pitch angle) comparison between the *FPID* and *GSFPID*. The error for *FPID* has high overshoot at time 5.8 sec but the *GSFPID* does not.

Figure 17 displays the pitch error comparison between *FPID* and *GSFPID* in boost phase. There is no steady state error for *GSFPID*.

Figure 18 depicts the pitch actuator (plant input) comparison between *FPID* and *GSFPID*. Figure 19 displays the pitch actuator comparison between *FPID* and *GSFPID* responses at first second in the boost phase.
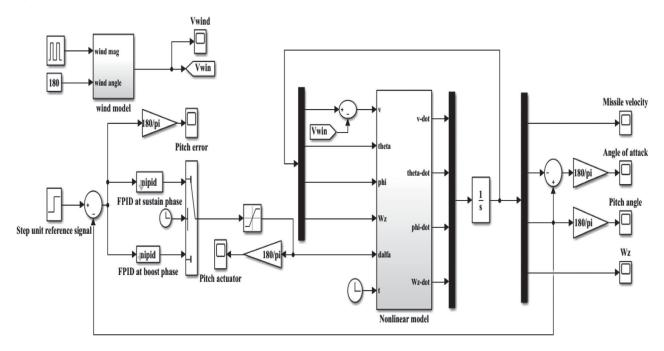

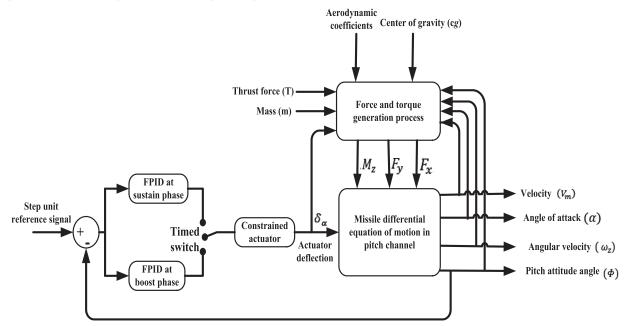**Figure 13.** Simulink diagram of nonlinear dynamic system with GSFPID in pitch channel.

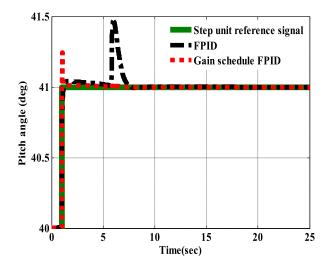**Figure 14.** Block diagram of nonlinear dynamic system with GSFPID in pitch Channel.
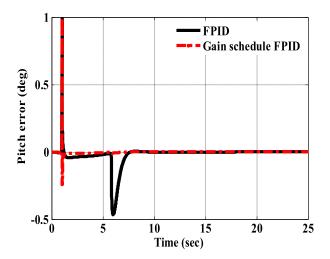
Figure 15. Pitch angle comparison.
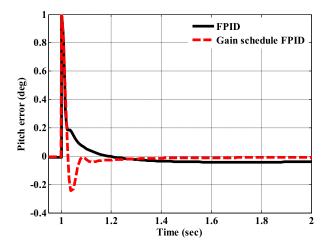

Figure 16. Pitch error comparison.

Figure 17. Pitch error comparison in boost phase.

Figure 18. Pitch actuator comparison.

Figure 19. Pitch actuator at first second in boost phase.

Figure 20. The missile velocity.

The down overshoot in *GSFPID* controller is less than that in *FPID* controller.

The missile velocity for *FPID* and *GSFPID* is given in Figure 20. The angle of attack for *FPID* and *GS FPID* controllers are shown in Figure 21
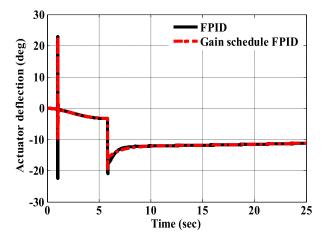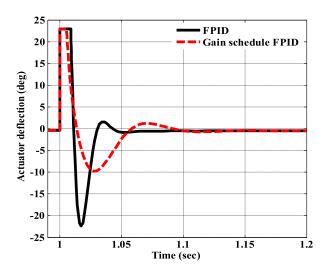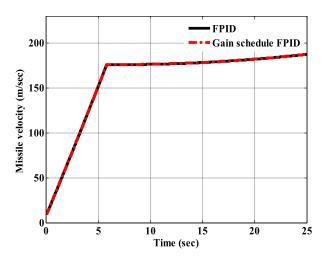
4.4. Wind effect

The wind effect is studied where wind velocity (that is presented in Figure 22) is summated to missile velocity (V_m) in the opposite direction and the results are compared. The profile of wind velocity was chosen from the horizontal wind model in Simulink library [28].
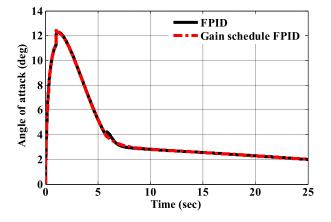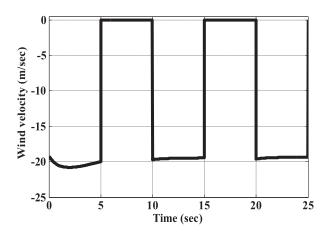
Figure 21. Angle of attack.
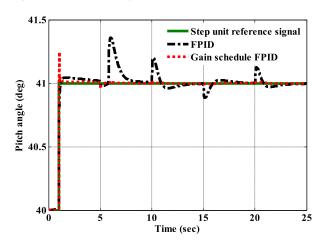

Figure 22. Wind velocity.

Figure 23. Pitch angle comparison with wind effect.

Figure 24. Pitch error comparison with wind effect.

Figure 25. Pitch actuator with wind effect.

Figure 26. Pitch angle comparison with 20% dynamic uncertain.

Figure 23 depicts the effect of wind on the pitch angle in *FPID* and *GSFPID*. The pitch angle with *FPID* gives the most change due to the wind effect. The pitch error with wind effect for *FPID* and *GSFPID* are shown in Figure 24.

Figure 25 displays the pitch actuator action due to the wind effect for *FPID* and *GSFPID* controller.

4.5. Dynamic uncertainty

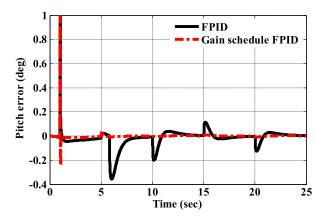In this section, the aerodynamic coefficients uncertainties are studied. The responses of *FPID* and *GSFPID* are compared during the change of the aerodynamic coefficient with 20% and 50%.

Figures 26–28 show the pitch angle, pitch error and pitch actuator comparison between *FPID* and *GSFPID* up to 20% dynamic uncertainties.

From the above figures, we can conclude that *FPID* and *GSFPID* cope with the change in aerodynamic coefficient up to 20%.

Figures 29 and 30 show the pitch angle and pitch actuator comparison between *FPID* and *GSFPID* up to 50% dynamic uncertainties. *GSFPID* cope with the change in aerodynamic coefficient up to 50% but *FPID* cannot because the pitch angle is out of control and

Figure 27. Pitch error comparison with 20% dynamic uncertain.
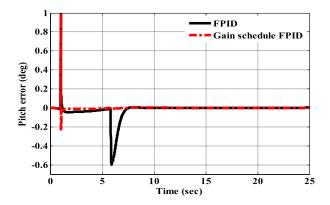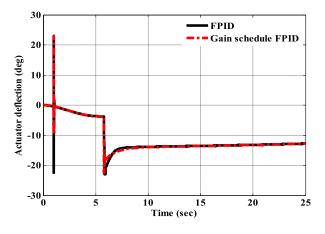

Figure 28. Pitch actuator comparison with 20% dynamic uncertain.
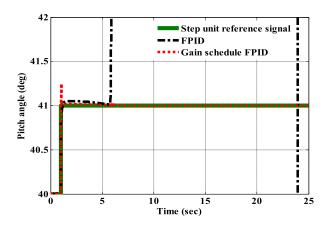

Figure 29. Pitch angle comparison with 50% dynamic uncertain.

the actuator deflection is saturated during the sustain phase.

4.6. Performance and stability

Many issues have to be considered in the analysis and design of control systems. The basic requirements are:

(1) Stability
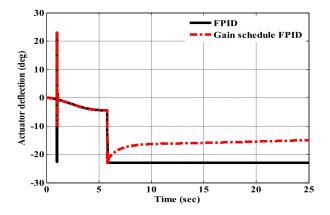(2) Ability to follow reference signals (performance)

Figure 30. Pitch actuator comparison with 50% dynamic uncertain.

(3) Reduction of effects of load disturbances (performance)
(4) Reduction of effects of model uncertainties (robustness)

Instability is the major drawback of feedback. Avoiding instability is thus a primary goal. It is also desirable that the process variable follows the reference signal. The system should also be able to reduce the effects of load disturbances. It must also be considered that the models used to design the control systems are inaccurate. The properties of the process may also change. The control system should be able to cope with moderate changes. In process control, the major emphasis is often on attenuation of load disturbances, while the ability to follow reference signals is the primary concern in motion control systems. In other cases, robustness may be the main requirement [37,38].

Figure 31 illustrates a stable system and an unstable system in Bode diagrams and polar plots [39].

The system is stable in the following cases:

- All poles of a linear system with negative real parts (i.e. all poles in the left-hand side in S-plane).
- The root locus in the Nyquist diagram of a linear system is not encirclement the point $-1 + j0$.
- The gain and phase margins in the Bode diagram of the linear system are positive.

In this section, the nonlinear closed-loop missile system is linearized by the Simulink linear analysis tool. The step response; Bode diagram; poles and zeros in S-plane; and Nyquist diagram are obtained by the Simulink linear analysis tool to study the performance and stability of the closed-loop linear system. The linearization occurs at the critical operating point $t = 5.8$ *sec* where this point separates between boost and sustain phases. Figure 32 depicts the step unit response for the closed-loop linear system.

FPID and *GSPID* controllers with the linear system can follow step unit response so they give a good

Figure 31. Phase and gain margins of stable and unstable systems (a) Bode diagrams (b) polar plots.

Figure 32. Step unit response for closed-loop linear system.

performance but *GSPID* control gives the best tracking and performance.

Figure 33 represents the Bode diagram for the closed-loop linear system.

The Nyquist diagram of the closed-loop linear system is displayed in Figure 34. The poles and zeroes for the closed-loop linear system in S-plane are given in Figure 35.

Bode Diagram

Figure 33. Bode diagram for closed-loop linear system.

Nyquist Diagram

Figure 34. The Nyquist diagram of closed-loop linear system.

Figure 35. Poles and zeroes of closed-loop linear system in S-plane.

The closed-loop linear system with *FPID* and *GSF-PID* are stable due to the following reasons:

- All poles on the left-hand side in S-plane as shown in Figure 35.
- The root locus in Nyquist diagram is not encirclement the point −1+*j*0 and fare away it as shown in Figure 34.
- The phase margin in the Bode diagram is positive as seen in Figure 33.

5. Conclusion and future work

5.1. Conclusion

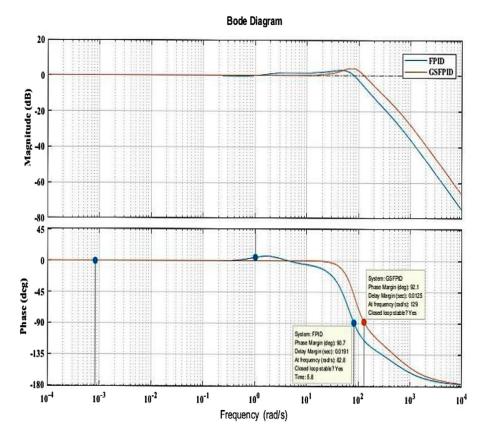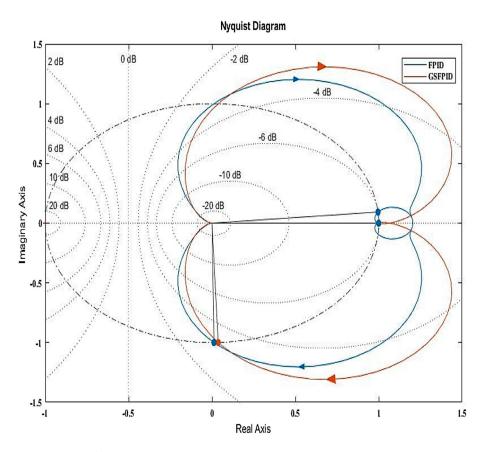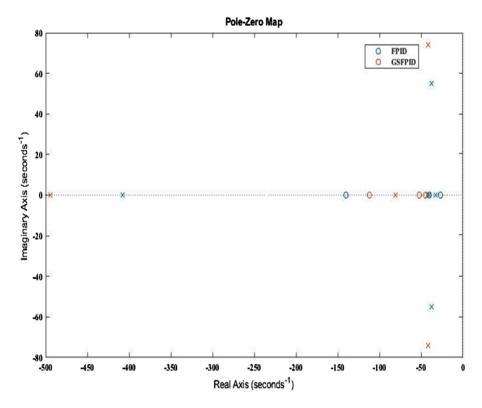In this paper, the flying of 6-*DOF* missile is simulated in the Simulink environment. *FPID* and *GSFPID* gains with nonlinear missile model simulation are tuned by Simulink design optimization. Simulink Design Optimization gives the best tuning parameters for *FPID* and *GSFPID*. The responses of *FPID* and *GSFPID* are compared. Pitch angle response with *FPID* and *GSF-PID* tracks step unit reference signal. *GSFPID* gives the best tracking where there is no steady state pitch error during boost phase and there is no overshoot at *t* = 5.8 sec (starting of sustain phase). The pitch actuator with *GSFPID* is the better response than *FPID* because the down overshoot at first second in boost phase is smaller than that in *FPID* controller. *GSF-PID* gives the best performance because pitch angle tracks pitch step unit response signal with nonlinear

missile model and with linear missile model at critical operating point *t* = 5.8 sec.

The responses with *GSFPID* are slightly changed due to wind effect. *FPID* can overcome plant dynamic uncertainties up to 20%. The plant with *FPID* at 50% dynamic uncertainty is out of control and actuator deflection is saturated during the sustain phase. *GSF-PID* can cope with plant dynamic uncertainties up to 50%. *GSFPID* with nonlinear missile model is a robust control because it can overcome the wind effect and plant dynamic uncertainties up to 50%. *FPID* and *GSF-PID* with the closed-loop linear system at critical operating point *t* = 5.8 sec are stable because of all their poles are on the left-hand side in S-plane and it has positive phase and gain margins. Finally, *GSFPID* controller gives the best performance, stability and the best deflection actuator. *GSFPID* controller is not affected by wind and it copes with dynamic uncertainties so it is more robustness.

5.2. Future work

In the future work, the control can be improved to make a further research. This includes designing a new controller such as Two-Dimensional Dissipative Control for Roesser Model that is presented in appendix A. other controllers can be studied such as model predictive control and *L*1 adaptive control. *GSFPID* control can also be applied to other nonlinear processes such as robotic arm control to obtain better controller performance characteristics. The containment control of

fractional order with linear time-varying (*LTV*) system will be investigated in future work. The control parameter can be tuned by using other optimization algorithms, like genetic algorithm, ant colony algorithm or immune algorithm to improve the control performance.

The proposed controller can be implemented in the real system such as the system-on-a-programmable-chip (*SoPC*) based hardware to achieve the online real-time control. *SoPC* is embedded with many logic gates, flip-flops, on-chip memory, and silicon intellectual property (*SIP*) for faster development of systems and lower cost of devices. Typically, this is realized in field programmable gate array (*FPGA*). *FPGA* is popular in industrial applications for its low cost, high speed, small size, and faster execution speed [40].

Disclosure statement

No potential conflict of interest was reported by the authors.

Funding

References

[1] Aboelela MA, Ahmed MF, Dorrah HT. Design of aerospace control systems using fractional PID controller. J Adv Res. 2012;3:225–232.

[2] Fawzy M, Aboelela M, El Rhman OA, et al. Design of missile control system using model predictive control. Online J Comp Sci Inform Technol. 2011;1:64–70.

[3] Wael MA, Quan Q. Robust hybrid control for ballistic missile longitudinal autopilot. Chin J Aeronaut. 2011;24:777–788.

[4] MacKenzie DA. Inventing accuracy: a historical sociology of nuclear missile guidance. Cambridge (MA): MIT press; 1993.

[5] Draper C. Guidance is forever. Navigation. 1971;18: 26–50.

[6] Spearman ML. Historical development of worldwide guided missiles. Hampton (VA): NASA Langley Research Center; 1983.

[7] Battin RH. Space guidance evolution – a personal narrative. J Guid Control Dyn. 1982;5:97–110.

[8] Fossier MW. The development of radar homing missiles. J Guid Control Dyn. 1984;7:641–651.

[9] Haeussermann W. Developments in the field of automatic guidance and control of rockets. J Guid Control Dyn. 1981;4:225–239.

[10] Locke AS. Guidance: principles of guided missile design. New York: Van Nostrand; 1955.

[11] Westrum R. Sidewinder: creative missile development at China Lake. Annapolis (MD): Naval Institute Press; 2013.

[12] Podlubny I, Dorcak L, Kostial I. On fractional derivatives, fractional-order dynamic systems and PIλDδ controllers. Proceedings of the 36th IEEE Conference on Decision and Control; San Diego, CA; 1997. p. 4985–4990.

[13] Suarez J, Vinagre B, Chen Y. Spatial path tracking of an autonomous industrial vehicle using fractional order

[14] Ferreira NF, Machado JT. Fractional-order hybrid control of robotic manipulators. Proceedings of the 11th International Conference on Advanced Robotics; Coimbra, Portugal; 2003.

[15] Reinecke M. Anti-stall hydraulic pump for a thrust vector control system. Google Patents, 2018.

[16] Zhao W, Wu B, Chen Q, et al. Fault-tolerant direct thrust force control for a dual inverter fed open-end winding linear vernier permanent-magnet motor using improved SVPWM. IEEE Trans Ind Electron. 2018;65:7458–7467.

[17] Blakelock JH. Automatic control of aircraft and missiles. Hoboken: John Wiley & Sons; 1991.

[18] Siouris GM. Missile guidance and control systems. New York: Springer Science & Business Media; 2004.

[19] Ashish T. Modern control design with Matlab and Simulink. Kanpur: John Wiley & Sons, Indian Institute of Technology; 2002.

[20] Siouris GM. Missile guidance and control systems: New York: Springer Science & Business Media; 2004.

[21] Basin MV, Yu P, Shtessel YB. Hypersonic missile adaptive sliding mode control using finite-and fixed-time observers. IEEE Trans Ind Electron. 2018;65:930–941.

[22] Garnell P, Qi Z, Xia Q. Guided weapon control systems. Beijing: Beijing institute of technology; 2003.

[23] Stevens BL, Lewis FL, Johnson EN. Aircraft control and simulation: dynamics, controls design, and autonomous systems. New York: John Wiley & Sons; 2015.

[24] Roskam J. Airplane flight dynamics and automatic flight controls. Lawrence (KS): DARcorporation; 1995.

[25] Cook MV. Flight dynamics principles: a linear systems approach to aircraft stability and control. Oxford: Butterworth-Heinemann; 2012.

[26] Agarwal RP, Baleanu D, Nieto JJ, et al. A survey on fuzzy fractional differential and optimal control nonlocal evolution equations. J Comput Appl Math. 2018;339: 3–29.

[27] Tyagi AK. Matlab and Simulink for engineers. Oxford: Oxford University Press; 2012.

[28] MathWorks I. Matlab: the language of technical computing. Desktop tools and development environment, version 7.10.0 Vol. 9. Natick (MA): MathWorks; 2010.

[29] Chapelle O, Wu M. Gradient descent optimization of smoothed information retrieval metrics. Inf Retr Boston. 2010;13:216–235.

[30] Cortés-Delgadillo B, Rodríguez-Navas PA, Guerrero-Linares LI, et al. Embedding Matlab Optimizers in SIMSIDES for the high-level design of sigma-delt Modulators. IEEE Trans Circuits Syst Express Briefs. 2018;65:547–551.

[31] Pradeepkannan SS. Implementation of gain scheduled PID controller for a nonlinear coupled spherical tank process. Int J Mech Mechatron Eng. 2014;14:6.

[32] Krishna M, Rao S, Raju R. Theoretical and experimental investigation of gain scheduling and adaptive autopilots for a model boat. Int J Eng Sci Technol. 2011;3:902–911.

[33] Araromi DO, Sulayman AA. Gain scheduling control design for shell heavy oil fractionator column. Int J Energy Environ Res. 2015;3(1):13–28.

[34] Donyanavard B, Rahmani AM, Muck T, et al. Gain scheduled control for nonlinear power management in CMPs. Design, Automation & Test in Europe Conference & Exhibition (DATE); Dresden, Germany; 2018. p. 921–924.

controllers. Proceedings of 11th International Conference on Advanced Robotics, ICAR; Coimbra, Portugal; 2003. p. 405–410.

[35] Hiramoto K, Matsuoka T, Sunakoda K. Adaptive gain scheduled semiactive vibration control using a neural network. Shock Vib. 2018;2018:1–19.

[36] MathWorks I. Matlab: the language of technical computing. Desktop tools and development environment, version 7 Vol. 9. Natick (MA): MathWorks; 2005.

[37] Zou C, Hu X, Dey S, et al. Nonlinear fractional-order estimator with guaranteed robustness and stability for lithium-ion batteries. IEEE Trans Ind Electron. 2018;65:5951–5961.

[38] Frank SA. Performance and robustness measures. In: Control theory tutorial. Irvine (CA): SpringerBriefs in Applied Sciences and Technology; 2018. p. 37–41.

[39] K. Ogata and Y. Yang. Modern control engineering. Upper Saddle River (NJ): Prentice Hall; 1970.

[40] Huang H-C, Tsai C-C. FPGA implementation of an embedded robust adaptive controller for autonomous omnidirectional mobile platform. IEEE Trans Ind Electron. 2009;56:1604–1616.

[41] Ahn CK, Shi P, Basin MV. Two-dimensional dissipative control and filtering for Roesser model. IEEE Trans Automat Contr. 2015;60:1745–1759.

[42] Du C, Xie L, Zhang C. H∞ control and robust stabilization of two-dimensional systems in Roesser models. Automatica. 2001;37:205–211.

[43] Wu L, Gao H. Sliding mode control of two-dimensional systems in Roesser model. IET Control Theory Applic. 2008;2:352–364.

[44] Sathishkumar M, Sakthivel R, Selvaraj P, et al. Robust reliable dissipative control of nonlinear networked control systems. Complexity. 2016;21:427–437.

[45] Ahn CK, Shi P, Basin MV. Deadbeat dissipative FIR Filtering. IEEE Trans Circuits Systems. 2016;63:1210–1221.

Appendix A. Two-dimensional dissipative control for Roesser model

In this appendix, we consider the 2-D dissipative control problems for the Roesser model with state-feedback controller based on Linear Matrix Inequality (*LMI*) approach. Consider the following 2-D model in the discrete time Roesser form:

$$x^h(i+1,j) = A_{11}x^h(i,j) + A_{12}x^v(i,j) + B_1u(i,j) \quad (A1)$$

$$x^v(i,j+1) = A_{21}x^h(i,j) + A_{22}x^v(i,j) + B_2u(i,j) \quad (A2)$$

$$y(i,j) = C_1x^h(i,j) + C_2x^v(i,j) + G_3w(i,j) \quad (A3)$$

$$z(i,j) = E_1x^h(i,j) + E_2x^v(i,j) + Fu(i,j) \quad (A4)$$

where $x^h(i,j) \in R^m$ is the horizontal state, $x^v(i,j) \in R^n$ is the vertical state, $u(i,j) \in R^p$ is the control input, $w(i,j) \in R^l$ is the external disturbance, $y(i,j) \in R^q$ is the output, and $z(i,j) \in R^r$ is the controlled output. $A_{11}, A_{12}, A_{21}, A_{22}, B_1, B_2, C_1, C_2, E_1, E_2, F, G_1, G_2, G_3,$ and G_4 are the system matrices.

Let us design the following state-feedback controller:

$$u(i,j) = K \begin{bmatrix} x^h(i,j) \\ x^v(i,j) \end{bmatrix} \quad (A5)$$

where $K = [K_1 \ K_2]$ is a controller gain. With this controller we obtain the following closed-loop system:

$$\begin{bmatrix} x^h(i+1,j) \\ x^v(i,j+1) \end{bmatrix} = (A + BK) \begin{bmatrix} x^h(i,j) \\ x^v(i,j) \end{bmatrix} + Gw(i,j) \quad (A6)$$

$$z(i,j) = (E + FK) \begin{bmatrix} x^h(i,j) \\ x^v(i,j) \end{bmatrix} + G_4w(i,j) \quad (A7)$$

where

$$G = \begin{bmatrix} G_1 \\ G_2 \end{bmatrix}, E = \begin{bmatrix} E_1 & E_2 \end{bmatrix}$$

Definition: (2-D (Q, S, R)-α Dissipative State Feedback Control) given some scalar $\alpha > 0$, matrices Q, S, and R with Q and R real symmetric, the controller (A5) is a 2-D (Q, S, R)-α dissipative state-feedback controller for any $T_i \geq 0$ and $T_j \geq 0$ if the following condition is satisfied under zero boundary conditions:

$$\sum_{i=0}^{T_i} \sum_{j=0}^{T_j} z^T(i,j)Qz(i,j) + 2\sum_{i=0}^{T_i} \sum_{j=0}^{T_j} z^T(i,j)Sw(i,j)$$

$$+ \sum_{i=0}^{T_i} \sum_{j=0}^{T_j} w^T(i,j)Rw(i,j) \geq \alpha \sum_{i=0}^{T_i} \sum_{j=0}^{T_j} w^T(i,j)w(i,j)$$

(A8)

More explanation about this subject is presented in [41–45].